Supplementary Materials

Mapping croplands in the granary of the Tibetan Plateau using all available Landsat imagery, a phenology-based approach and Google Earth Engine

Di, et al.

Includes:

Figures S1-11

Tables S1

References

Figure S1. Number of good observations at the pixel level during the growing season (April-October) from 2015 to 2019 in the study area.

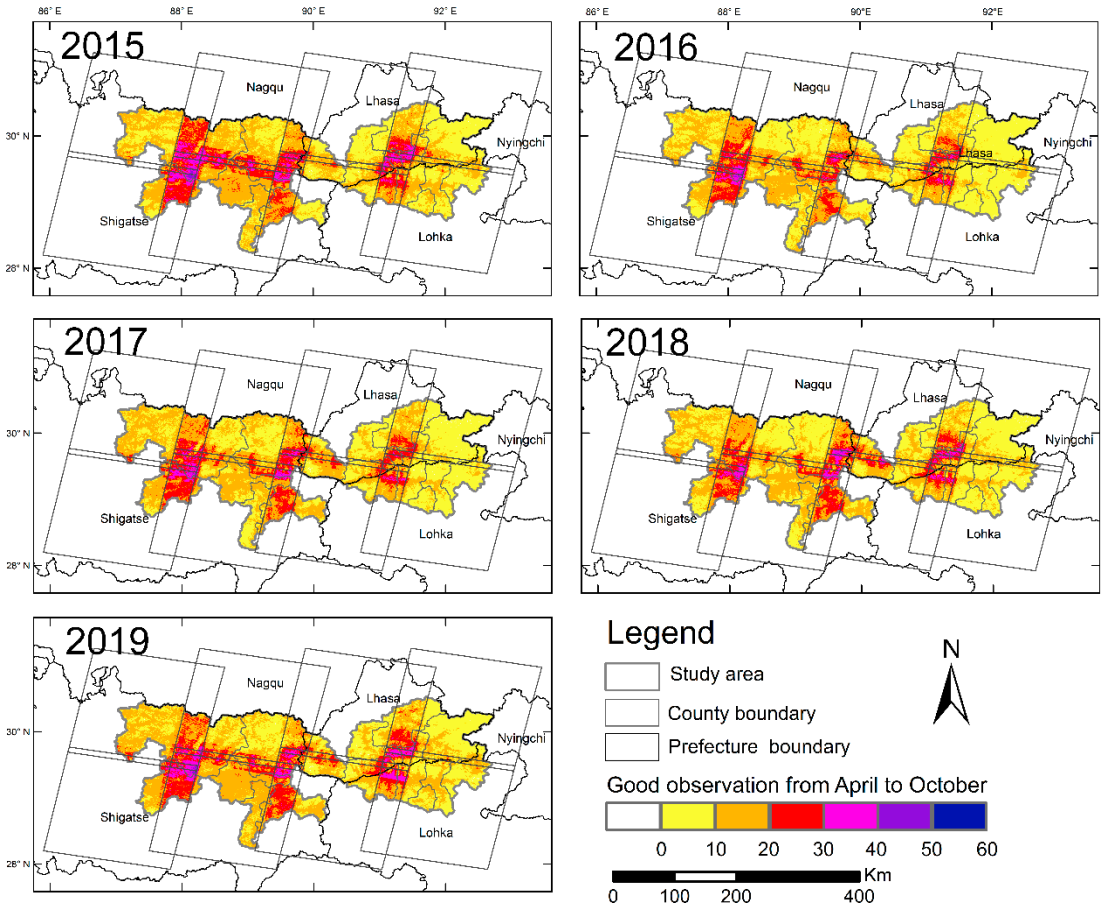

Figure S2. Field photo, Google Earth high-resolution imagery, and Landsat false-color composite imagery of five land-use types. The false-color imagery (R: near-infrared, G: red, B: green) was composited in July and October.

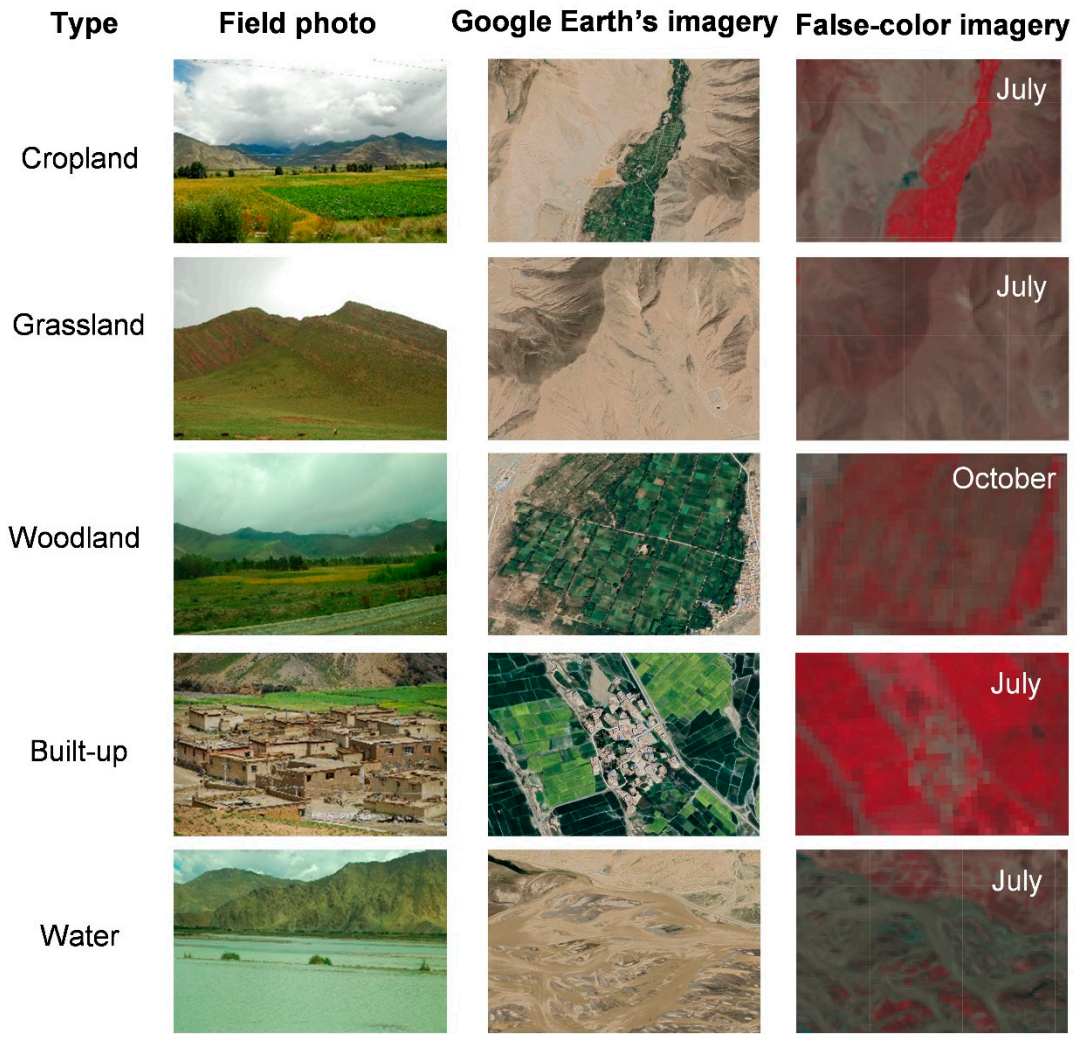

Figure S3. Spatial distributions of the training points of interests (POIs) of five land-use types (cropland, grassland, woodland, water, and built-up). The background is the world terrain base map.

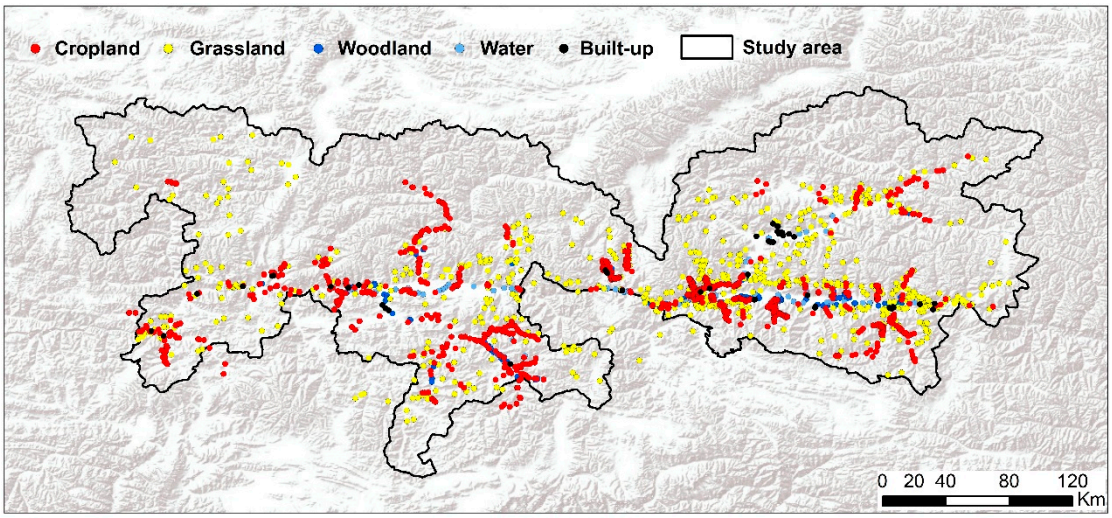

Figure S4. Landsat false-color composite imagery (R: near-infrared, G: red, B: green) of croplands from April to October at four elevation gradients.

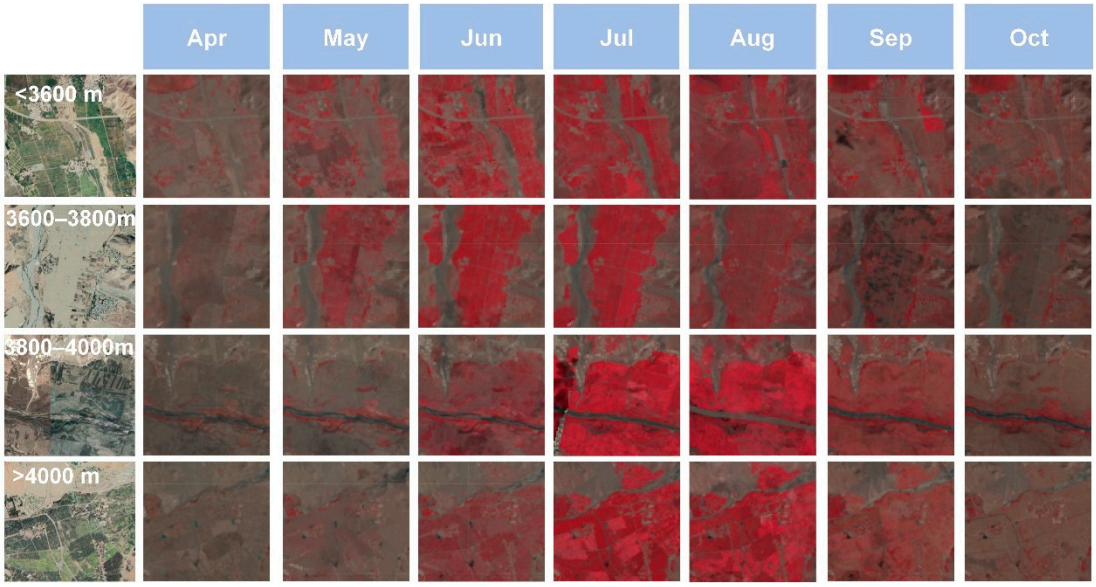

Figure S5. Monthly mean and standard deviation (SD) of Normalized Difference Vegetation Index (NDVI) for five land-use types based on the training POIs over years of 2015-2019. The orange shadow shows the period used to distinguish the vegetated area from water and built-up.

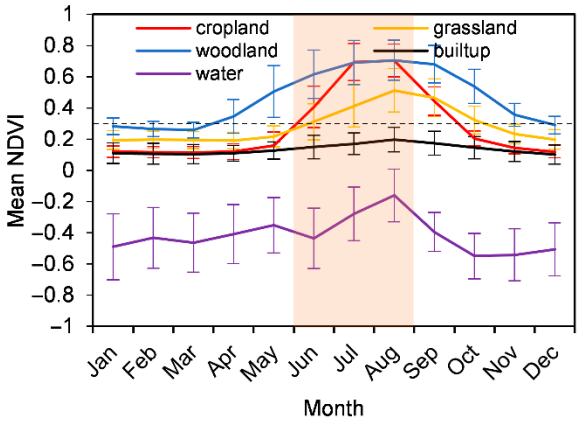

Figure S6. Number of good observations at the pixel level in July from 2015 to 2019 and total good observations over 2015-2019 in the study area.

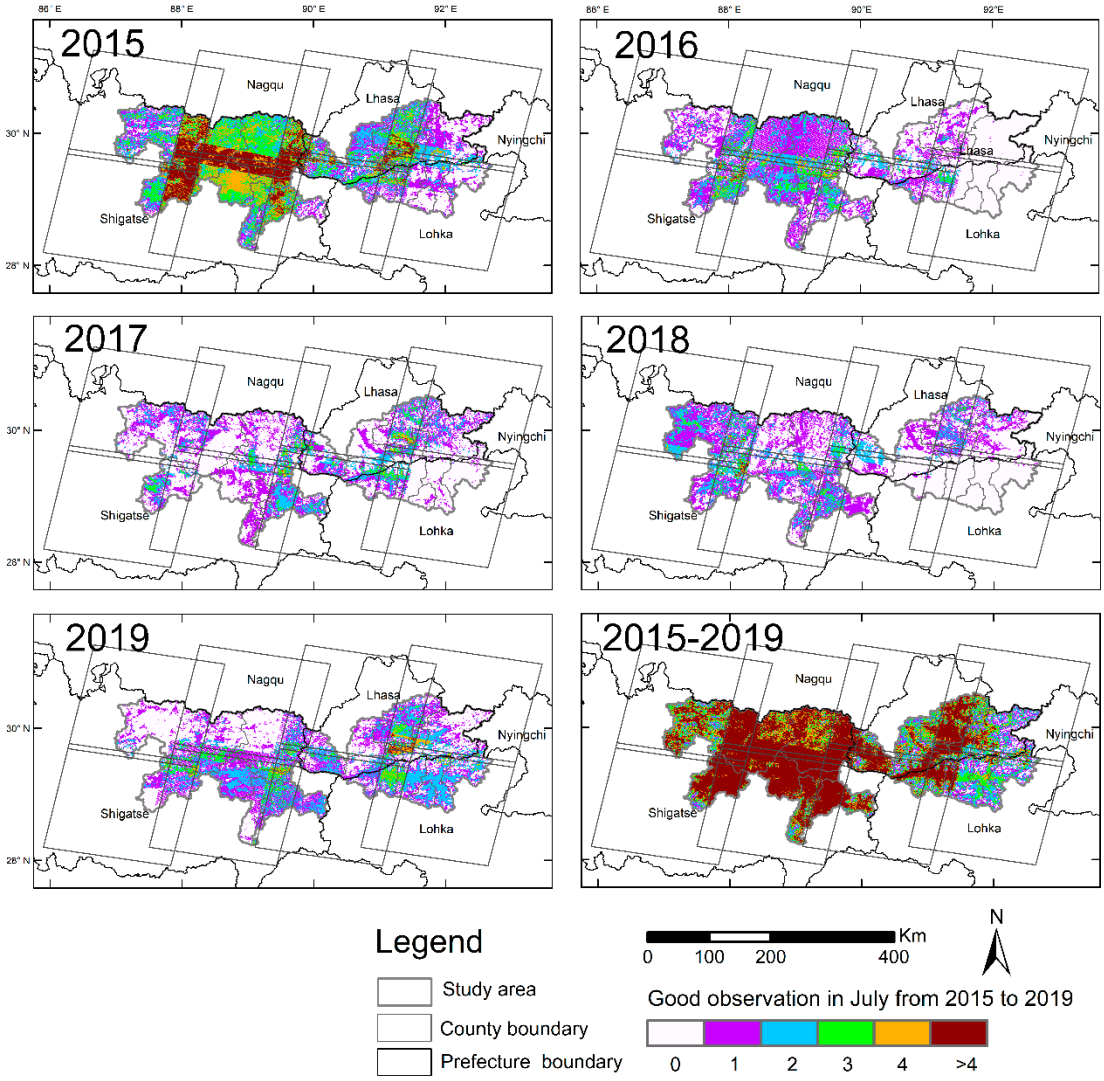

Figure S7. Number of good observations at the pixel level in August from 2015 to 2019 and total good observations over 2015-2019 in the study area.

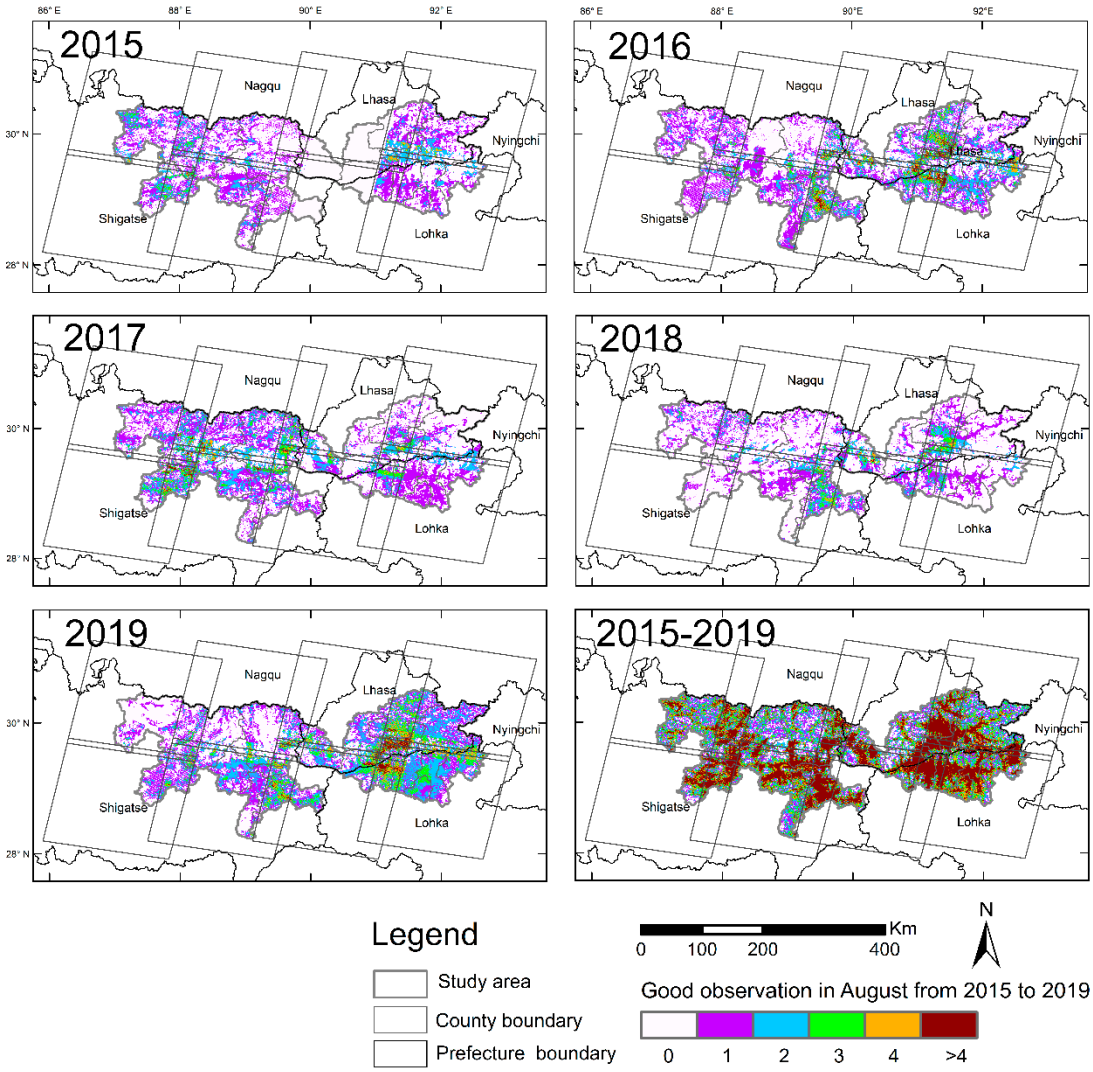

Figure S8. Monthly mean and standard deviation (SD) of Normalized Difference Vegetation Index (NDVI), Enhanced Vegetation Index (EVI), and Land Surface Water Index (LSWI) of cropland, grassland, and woodland based on the training POIs over years 2015-2019.

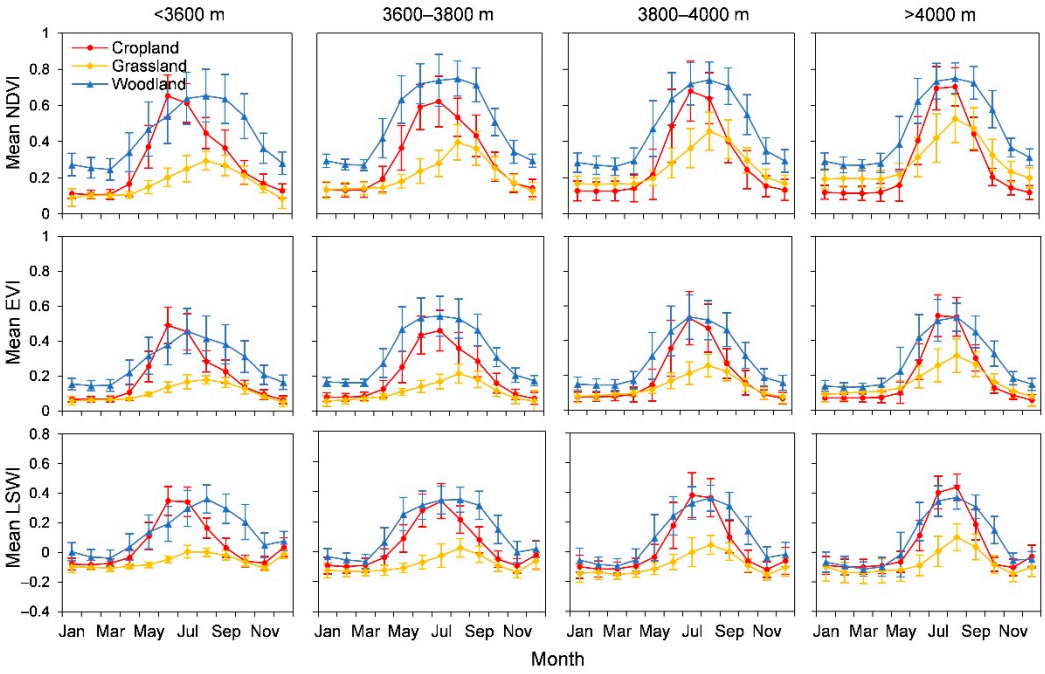

Figure S9. (a) The spatial distribution of croplands in the late 2010s derived from the PCM1 (2015-2019) and PCM2 (2017-2019) in the study area. (b-e) are the zoom-in views of four regions labeled as (1-4) in (a), respectively.

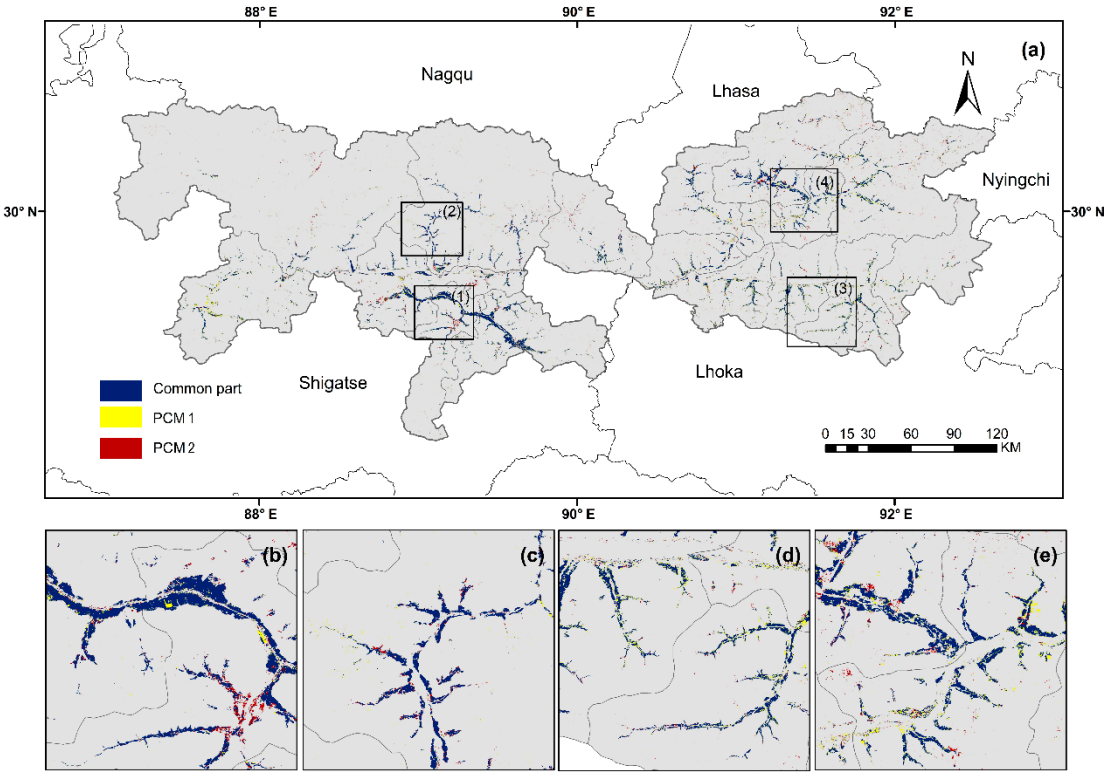

Figure S10. Comparison of the cropland maps produced using the second Phenology-based Cropland Mapping (PCM2) algorithm in this study and China's Land-Use/cover Datasets (CLUDs) in 2015. (a-c) are the zoom-in views of three regions labeled as (1-3) in the top figure, respectively. (d) The cropland area and the common area based on two cropland maps. (e), (i), and (k) are the zoom-in views of three regions in (a-c) respectively. (j) and (l) are the time series of vegetation indices at selected sites in (i) and (k), respectively.

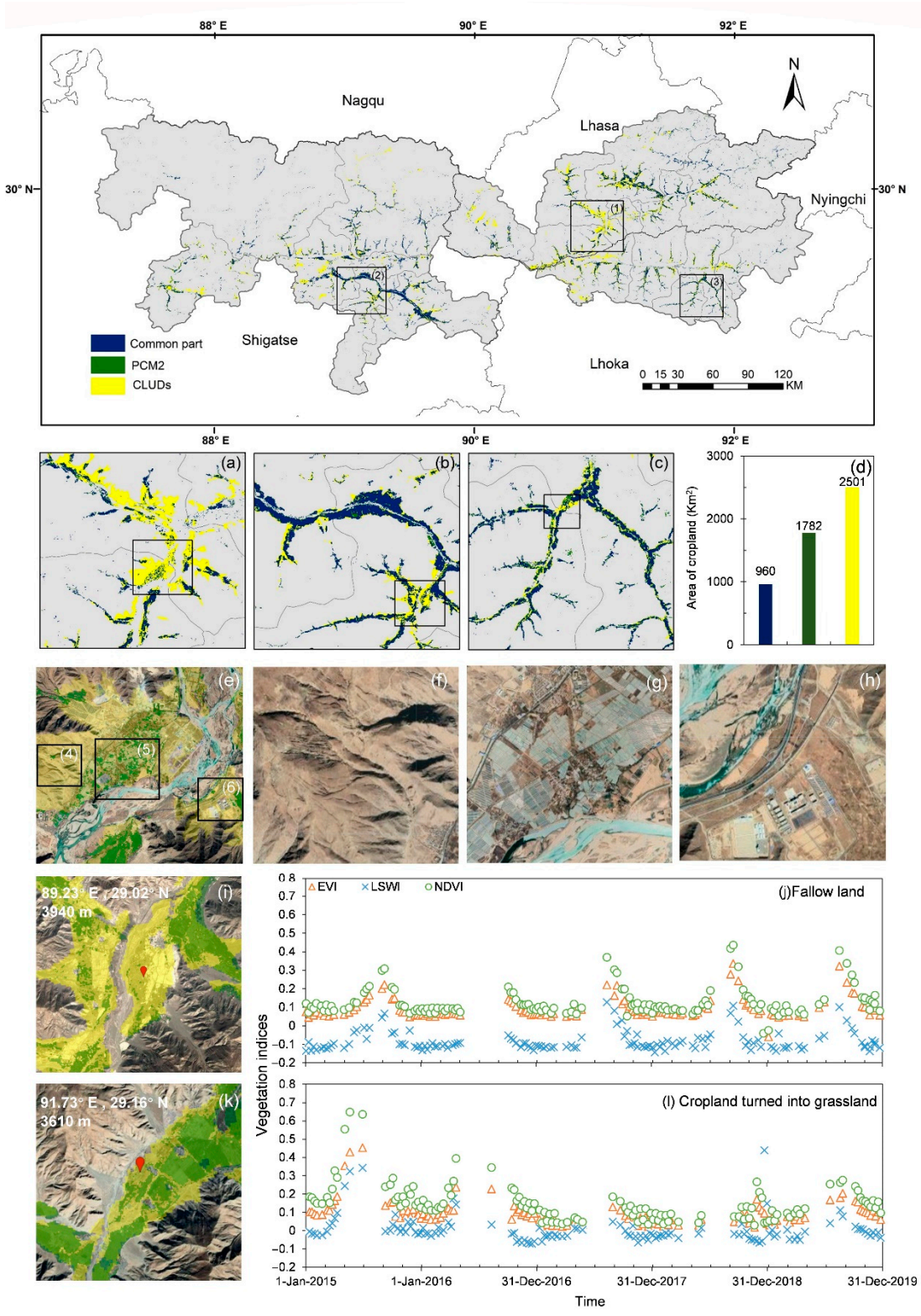

Figure S11. Cropland maps based on the first phenology-based cropland mapping (PCM1) algorithm composited imagery from one to five (a-f) years.

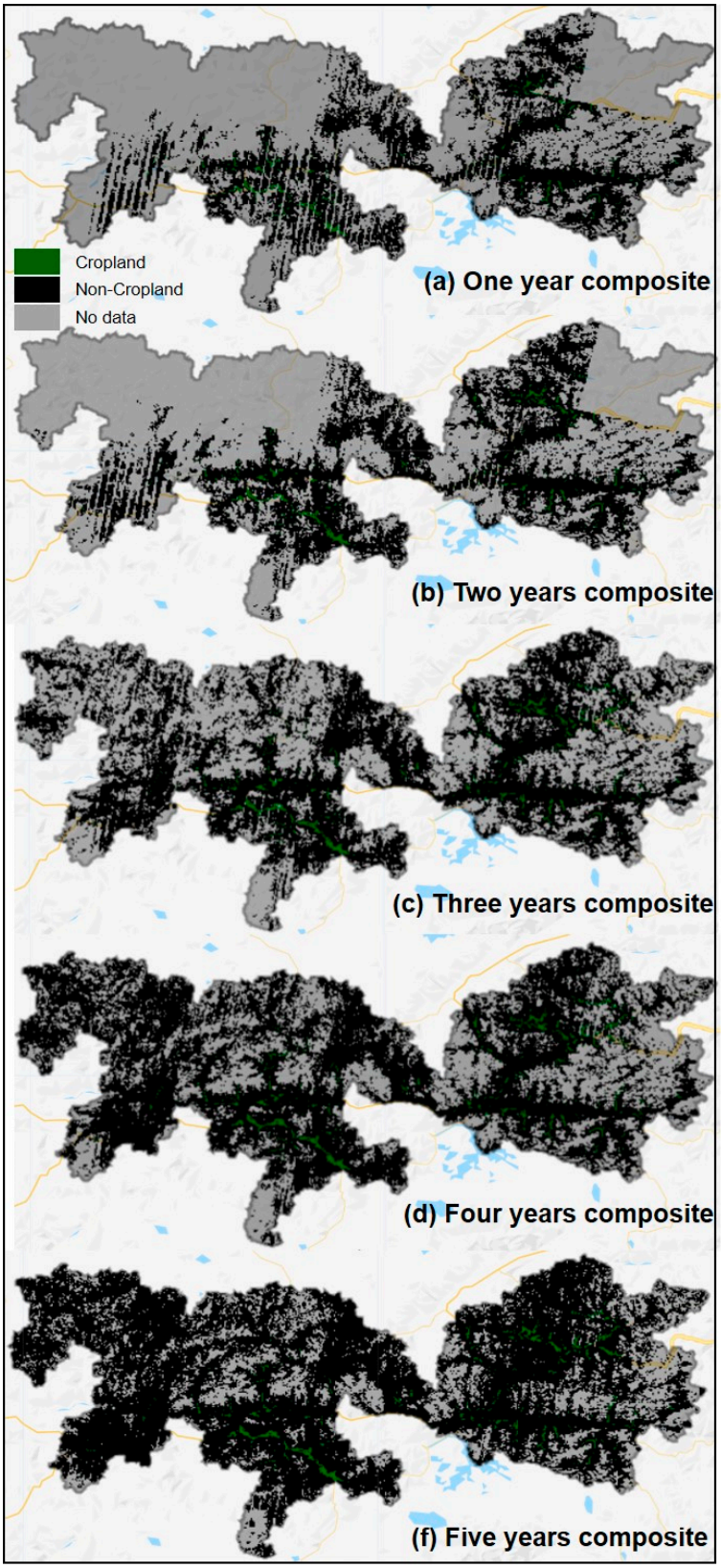

Table S1. Confusion matrix of cropland map based on the validation AOIs from high-resolution images from Google Earth and China's Land-Use/cover Datasets (CLUDs) in 2015.

Methods		Ground truth pixels		Classified pixels
		Cropland	Non-Cropland	
PCM1	Cropland	627	50	677
	Non-Cropland	107	7062	7169
	Sample total	734	7112	7846
PCM2	Cropland	694	70	764
	Non-Cropland	56	10002	10058
	Sample total	750	10072	10822